



# Evaluation of Winkler Model and Pasternak Model for Dynamic Soil-Structure Interaction Analysis of Structures Partially Embedded in Soils

Ting Bao<sup>1</sup> and Zhen “Leo” Liu, Ph.D.<sup>2</sup>

**Abstract:** This paper reports a comprehensive study including detailed experimental, theoretical, and numerical analyses to evaluate the performance of two predominant soil-structure interaction models, that is, the Winkler model and Pasternak model, in predicting the predominant natural frequency (PNF) of structures partially embedded in soils. For the evaluation, PNF-based scour detection, a nondestructive testing technique that has been receiving increasing attention, was adopted. First, a series of lab experiments was conducted using idealized piers partially embedded in two representative soils, that is, a sand and a clay, to measure the PNF-scour depth relationship. Next, a mathematical model was established and numerically implemented to predict the PNF of the idealized piers for scour detection. The soil-structure interaction was formulated using the Winkler model, which only considers the modulus of subgrade reaction for soils, and the Pasternak model, which considers the shear interaction in addition to the modulus. The numerically computed PNFs were then compared with those from the experiments in this study and a documented field test. Our results clearly show that when structures are partially embedded in soils, the Winkler model yields a better PNF prediction than the Pasternak model, regardless of the types of test piers and soils. This finding is different from those obtained in the dynamic response of structures resting on or fully embedded in an elastic foundation (i.e., not partially embedded), where the Pasternak model yields more realistic results than the Winkler model because of its consideration of the continuity of foundation media via the shear interaction. Because of the shear interaction, the PNFs predicted with the Pasternak model in this study are about 24%–38% and 31%–39% higher than the predictions with the Winkler model and the measured PNFs, respectively. DOI: 10.1061/(ASCE)GM.1943-5622.0001519. © 2019 American Society of Civil Engineers.

**Author keywords:** Predominant natural frequency; Scour detection; Winkler soil-structure interaction; Pasternak soil-structure interaction; Shear interaction.

## Introduction

The dynamic behavior of structures with soil-structure interaction (SSI) is a significant consideration in the design of structures, especially those subjected to dynamic loads from blasting waves (Huang et al. 2011), earthquakes (Far et al. 2013), wind actions (Lombardi et al. 2013), and so on. Understanding SSI is also critical to structural health monitoring that is based on the dynamic responses of structures (e.g., natural frequency). Because of SSI, the dynamic responses of structures are very sensitive to soil material properties (e.g., soil stiffness). Taking the frequency-based scour detection, for example, scour severity around bridge foundations can be detected by investigating changes in the predominant natural frequency (PNF) of a bridge or bridge component such as a pier (Ju 2013; Prendergast et al. 2013; Bao and Liu 2016). Progressive scour reduces the stiffness of a bridge pier because of the loss of support from the surrounding soils, which causes the PNF to decrease. The progression of scour, in fact, reduces the interaction

between the pier and soils by removing soils around the pier, leading to changes in SSI during the scour development. As a result, it is vital for accurately modeling dynamic SSI to obtain accurate PNFs for such an application as well as any other structural health monitoring applications involving dynamic SSI.

Because of the importance of SSI, many research efforts have been made to understand and characterize the dynamic responses of a test structure involving SSI, for example, Gerolymos and Gazetas (2006), Liu et al. (2014), and Hussien et al. (2018). The  $p$ - $y$  curve is an acceptable approach to obtain the soil stiffness in SSI, which has been verified by field test results with different soils (Matlock 1970; Cox et al. 1974; Reese and Welch 1975) and pile groups (Taghavi and Muraleetharan 2016). This approach has also been applied to structural health monitoring, particularly the previously introduced frequency-based bridge scour detection, where bridge piers are partially embedded in soils. Prendergast et al. (2013) performed simulations of an idealized pier embedded in soils as a beam partially embedded in an elastic foundation to detect progressive scour in terms of the PNF of that pier. Other researchers, for example, Ko et al. (2010) and Foti and Sabia (2011), investigated the influence of scour progression on the dynamic responses of a bridge using the sprung-beam elements to represent SSI. Also, Ju (2013) developed numerical methods to compute the PNF for scour detection by accounting for SSI with the effective mass theory. These studies were mostly conducted directly or indirectly based on a simple model, that is, the Winkler model, for formulating dynamic SSI.

However, no research has been reported on the effectiveness of existing SSI formulations for a typical dynamic scenario: the frequency of a structure partially embedded in the soil. In addition to

<sup>1</sup>Research Associate, Dept. of Civil and Environmental Engineering, Michigan Technological Univ., 1400 Townsend Dr., Dow 854, Houghton, MI 49931. Email: tbao@mtu.edu

<sup>2</sup>Associate Professor, Dept. of Civil and Environmental Engineering, Michigan Technological Univ., 1400 Townsend Dr., Dillman 201F, Houghton, MI 49931 (corresponding author). Email: zhenl@mtu.edu

Note. This manuscript was submitted on July 15, 2018; approved on April 29, 2019; published online on December 9, 2019. Discussion period open until May 9, 2020; separate discussions must be submitted for individual papers. This paper is part of the *International Journal of Geomechanics*, © ASCE, ISSN 1532-3641.

the Winkler model, a comprehensive review conducted by Dutta and Roy (2002) summarized many methods for formulating SSI in addition to the Winkler model. Among them, the Pasternak model is deemed an improved version of the Winkler model by adding the shear interaction between the spring elements in order to consider more realistic soil characteristics (i.e., continuity of foundation media). Because of this change, the Pasternak model yields more realistic results compared to the Winkler model for the dynamic response of structures resting on an elastic foundation by additionally considering the continuity of the nature of foundation media (Dutta and Roy 2002). Also, the comparison results (Wang et al. 2014, 2017) showed that the Pasternak model is more accurate than the Winkler model for analyzing the dynamic responses of piles fully embedded in soils. As a result, the Pasternak model has been used in many studies to formulate SSI for obtaining the dynamic response of structures resting on or fully embedded in an elastic foundation (Valsangkar and Pradhanang 1988; De Rosa and Maurizi 1998; Wang et al. 2014). A detailed summary regarding the free vibration of beams resting on the Pasternak foundation can be found in Lee et al. (2014). However, no study has been reported on analyzing the PNF of structures (e.g., bridge piers) partially embedded in soils (i.e., not resting on or fully embedded) with the Pasternak model. Therefore, there is still an urgent need to evaluate the Pasternak model for analyzing the dynamic responses of structures partially embedded in soils.

In addition, in the application of frequency-based scour monitoring, numerical methods are preferable for complicated bridge structures (Ko et al. 2010; Foti and Sabia 2011; Prendergast et al. 2013; Prendergast and Gavin 2016). However, detailed procedures for a straightforward and easily implementable numerical framework for calculating the PNF with detailed SSI are still absent in the literature. Prendergast et al. (2013) performed simulations using MATLAB code for PNF-based scour detection. A following study (Prendergast and Gavin 2016) investigated the influence of coefficients of subgrade reaction models on the predicted PNFs. However, a comprehensive theoretical model involving SSI and details about its numerical implementations are lacking.

To advance the topic, in this study, we evaluate two SSI formulations, that is, the Winkler model and the Pasternak model, for dynamic modeling in predicting the PNF of a structure partially embedded in the soil. For the evaluation, PNF-based scour detection was adopted as the application to assist in our evaluation. The main goal is to evaluate which SSI formulation yields a better prediction of PNFs for scour detection. To achieve this goal, a series of lab-scale tests was conducted first using idealized piers partially embedded in typical less cohesive soils (sands) and cohesive soils (clays) to cover two representative types of soils at most bridges. A numerical framework was then developed with a comprehensive governing equation for an idealized beam partially embedded in a semiinfinite linear elastic medium. Detailed procedures for implementing the numerical framework were presented. Finally, the PNFs calculated based on the Winkler and Pasternak SSI formulations were discussed and compared with the experimental results in this study and those from a documented field test.

## Experiments

### Experiment Setup

Prendergast et al. (2013) conducted multiple experimental studies to investigate the change in the PNF of an idealized pier for scour detection. The study of Prendergast et al. (2013) served as a preliminary assessment and provided a simple method for the subsequent investigations of PNF-based scour detection. Based on the study of Prendergast et al. (2013), in the current study, a lab-scale model with idealized piers was constructed to assess the dynamic response of piers partially embedded in a soil block. Lab-scale tests were performed based on previous studies (Shinoda et al. 2008; Prendergast et al. 2013) by installing an accelerometer on the piers. Data measured by the accelerometer were transformed from the time domain to the frequency domain to obtain the PNF using the fast Fourier transform (FFT). Different geometric configurations and materials were adopted for the test piers to represent different pier types. The geometric properties are detailed in Table 1. The geometric similarity ratio can be calculated using either test diameter/real diameter or test length/real length (test diameter/real diameter = test length/real length) based on the typical dimensions of the piles. Both the steel rod and hollow pipe have the same ratio of 1/11. A similar two structures will be used for dynamic modeling in the later section.

Two types of soils, that is, a sand and clay, were used for the test to consider two major representative SSI scenarios at most bridges. The sand was uniform with almost the same grading, which is a typical sand collected at a riverbed to represent less cohesive soils. The clay had medium plasticity, which is a typical clay collected at a landslide site near a river to represent cohesive soils. The scales were marked on the test piers to easily read scour depths [Fig. 1(a)]. The soils were compacted layer by layer in increments of 150 mm, in which the sand was compacted to an approximate 100% relative density. The soils were housed in a plastic tank with dimensions of 520, 855, and 1,280 mm in depth, width, and length, respectively.

The accelerometer was mounted at a location that was very close (10 mm) to the top of the piers to record dynamic data based on the previous study in Bao et al. (2017), as shown in Figs. 1(a and b). The accelerometer (PCB model type: 333B30, PCB Piezotronics, Depew, New York) has a sensitivity of 10.2 mV/(m/s<sup>2</sup>), frequency range of 0.5–3,000 Hz, measurement range of ±490 (m/s<sup>2</sup> pk), broadband resolution of 0.0015 (m/s<sup>2</sup> rms), and spectral noise of 14 (μm/s<sup>2</sup>)/√Hz. The accelerometer and a modal hammer were connected to a data acquisition system to collect dynamic data, as shown in Fig. 1(c). The modal hammer (PCB model type: 086D05, PCB Piezotronics, Depew, New York) had a sensitivity of 0.23 mV/N and measurement range of ±22,240 N pk. The modal hammer was used to generate vibration by applying a transient force on the plane where the accelerometer was fixed. Dynamic signals of the pier and transient force were recorded by the data acquisition system after the transient force was applied. The data acquisition system included a PicoScope 3205 oscilloscope and a PCB 442C04 4-channel sensor signal conditioner (PCB Piezotronics, Depew, New York). The oscilloscope had a maximum sampling rate of 500 MS/s, analog-to-digital

**Table 1.** Geometries of the idealized piers and initial scour situations

Test pier	Height (mm)	Width/length (mm)	Diameter (mm)	Embedded length (sand/clay) (mm)	Scour increment (mm)	Soil compactness
Concrete column	306	—	153	226/156	20	High
Concrete brick	406	77/100	—	236/166	20	High
Steel rod	1,640	—	25	300/250	20	High
Hollow pipe	1,610	—	49/51 (inter/outer)	290/260	20	High

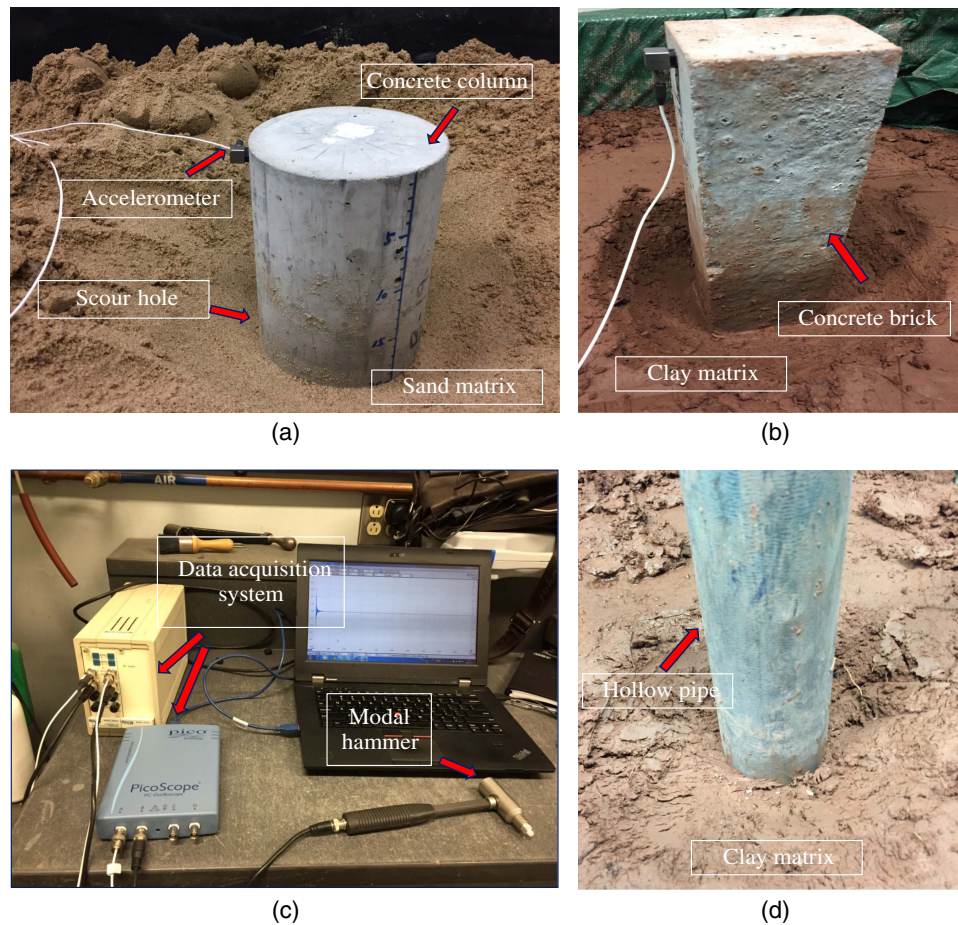


**Fig. 1.** Laboratory scour test: (a) concrete column in the sand; (b) concrete brick in the clay; (c) data collection; and (d) hollow pipe in the clay.

converter (ADC) effective number of 7.6 bits, and less than 0.01 Hz for the frequency resolution of output signals. The signal conditioner had a sensor excitation voltage of  $25.5 \text{ V} \pm 1.5 \text{ V}$ , frequency response of 5% (Hz/kHz), and spectral noise of  $0.57 (\mu\text{V})/\sqrt{\text{Hz}}$ . To obtain enough data for postprocessing, the system was established to work at a scanning frequency of 3,000 Hz.

Different scour depths were produced by removing soils around the test piers, in which an increment of 20 mm was used, as presented in Figs. 1(a, b, and d). Scour holes were symmetrical and constructed to be a cone shape. The initial scour level (Level 1) corresponded to the situation of no scour hole around the pier. The Scour level 6 was the final scour depth for each test pier, for which five layers of soil had been removed. The scour conditions adopted in the experiment are detailed in Table 1. The schematic of the geometry of the test piers is shown in Fig. 2. The simulation results concluded by Ju (2013) for the full-scale bridge showed that the difference in the PNFs calculated with and without the fluid-structure interaction was negligible. Therefore, the effect of the fluid-structure interaction was assumed to be negligible in this study. However, soils around a bridge pier, in reality, are always under water. In order to reflect this situation, water was added into the soil matrices, and the gravimetric water contents of the sand and clay were 4% and 23%, respectively.

### Laboratory Test Results

The impulse force, which was applied to the piers in the test, was analyzed to understand its frequency spectrum and the duration of

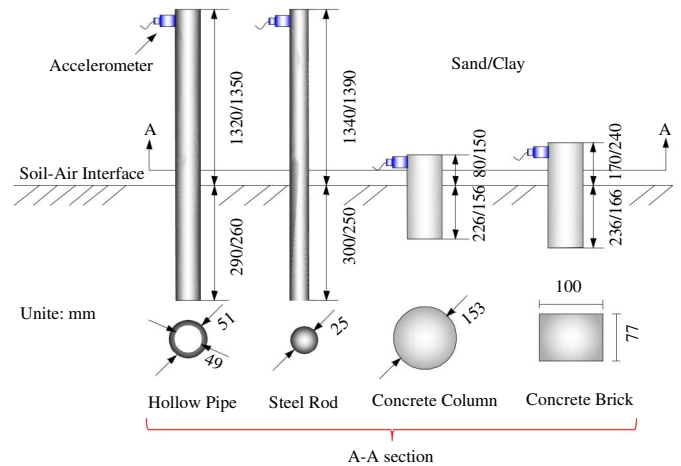


**Fig. 2.** Schematic of the geometry of test piers.

contact between the hammer and pier. This is because the impulse force determines the magnitude of negative effects generated by the hammer on the measured PNF (Shinoda et al. 2008; Foti and Sabia 2011). The evaluation results indicated that the transient impulse force, which was adopted in this study, is an ideal impulse force as described in Shinoda et al. (2008). The contact duration was around 1.8 ms, and almost a constant frequency amplitude was maintained within the duration, which is similar to the results in the study of Bao et al. (2017).

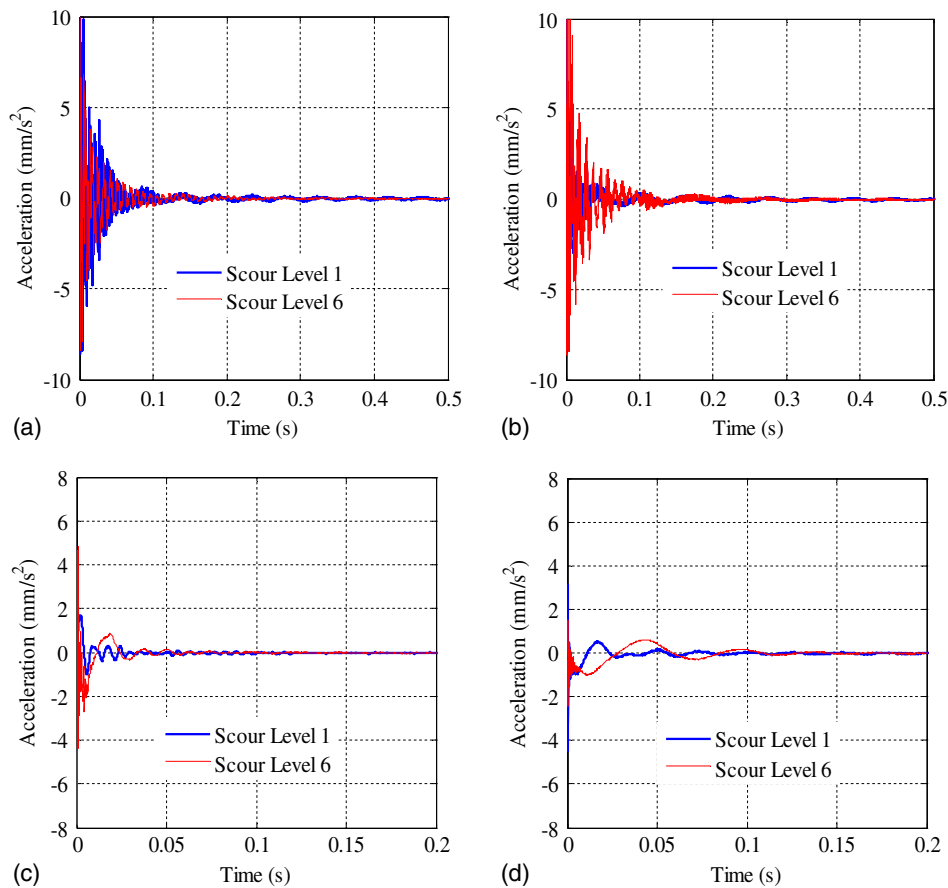


**Fig. 3.** Measured acceleration at (a) Scour levels 1 and 6 of the hollow pipe in the sand; and (b) clay; Scour levels 1 and 6 of the concrete column in the (c) sand; and (d) clay.

The measured dynamic responses of the hollow pipe and concrete column in terms of acceleration in the sand and clay at Scour levels 1 and 6 are shown in Fig. 3. The acceleration contained a significant amount of high-frequency vibration, including assembled and superposed waveforms due to local effects (Roy and Ganesan 1995; Prendergast et al. 2013). However, the PNF of the pier was usually in the low-frequency range, which is irrelevant to those high frequencies. Therefore, a low-pass filter was applied to filter the signals of acceleration in Fig. 3. A similar approach for postprocessing dynamic signals was also applied in the study of Prendergast et al. (2013). The filtered signals of the hollow pipe are shown in Figs. 4(a and b). The results clearly show that the periods in the filtered signal of Scour level 6 are significantly larger than those of Scour level 1 because of a greater scour depth. Similar results were also obtained in the filtered signals of the concrete column. As shown in Figs. 4(c and d), the periods in the filtered signal of Scour level 6 are obviously greater than those of Scour level 1.

To obtain the PNF at each scour level, the FFT was used to transfer the dynamic signals from the time domain to the frequency domain. As shown in Fig. 5(a), the PNF of the hollow pipe decreased from 20.5 (Level 1) to 14.2 Hz (Level 6) in the sand matrix. The PNF decreased from 17.6 to 10.5 Hz in the clay matrix. The PNF of the concrete column also decreased from 130.6 (Level 1) to 51 Hz (Level 6) in the sand and decreased from 37 to 19.2 Hz in the clay [Fig. 5(b)]. In all these tests, there is a clear reduction in the PNF with an increase of the scour depth, regardless of the types of piers and soils [Figs. 5(c and d)].

## Numerical Analysis

### Mathematical Model

In this section, a numerical framework was developed to simulate the previous lab-scale tests. Two widely used methods for the SSI formulation, that is, the Winkler model and the Pasternak model, were adopted for calculating the PNF. The Pasternak model is an improved version of the Winkler model by simulating an elastic foundation with two foundation parameters (Wang et al. 2001; Chen et al. 2004). To be more specific, it involves the shear interaction between the spring elements by adding a shear layer connecting the ends of the springs to a beam or a plate (Dutta and Roy 2002). The two foundation parameters are the modulus of subgrade reaction (Winkler parameter) and the Pasternak parameter. The latter is related to the shear modulus of the shear layer in the soil media (Wang et al. 2013).

The Pasternak model has been widely used to investigate vibration of beams on an elastic foundation (Yokoyama 1991; De Rosa 1995; Chen et al. 2004). The hypothesis of the Pasternak model is that soils can be represented as a series of unconnected and concentrated springs perpendicular to the pier with the shear interaction between the spring elements (Dutta and Roy 2002), which is considered using a shear layer (Fig. 6). The test pier embedded in the soils is modeled using a series of beam elements. For the Winkler SSI, it can be easily achieved by directly removing the shear layer. In this section, the hollow pipe and steel rod used in the previous lab-scale tests were selected for the simulation. The conceptual models used to simulate the lab-scale tests are shown in Fig. 6.

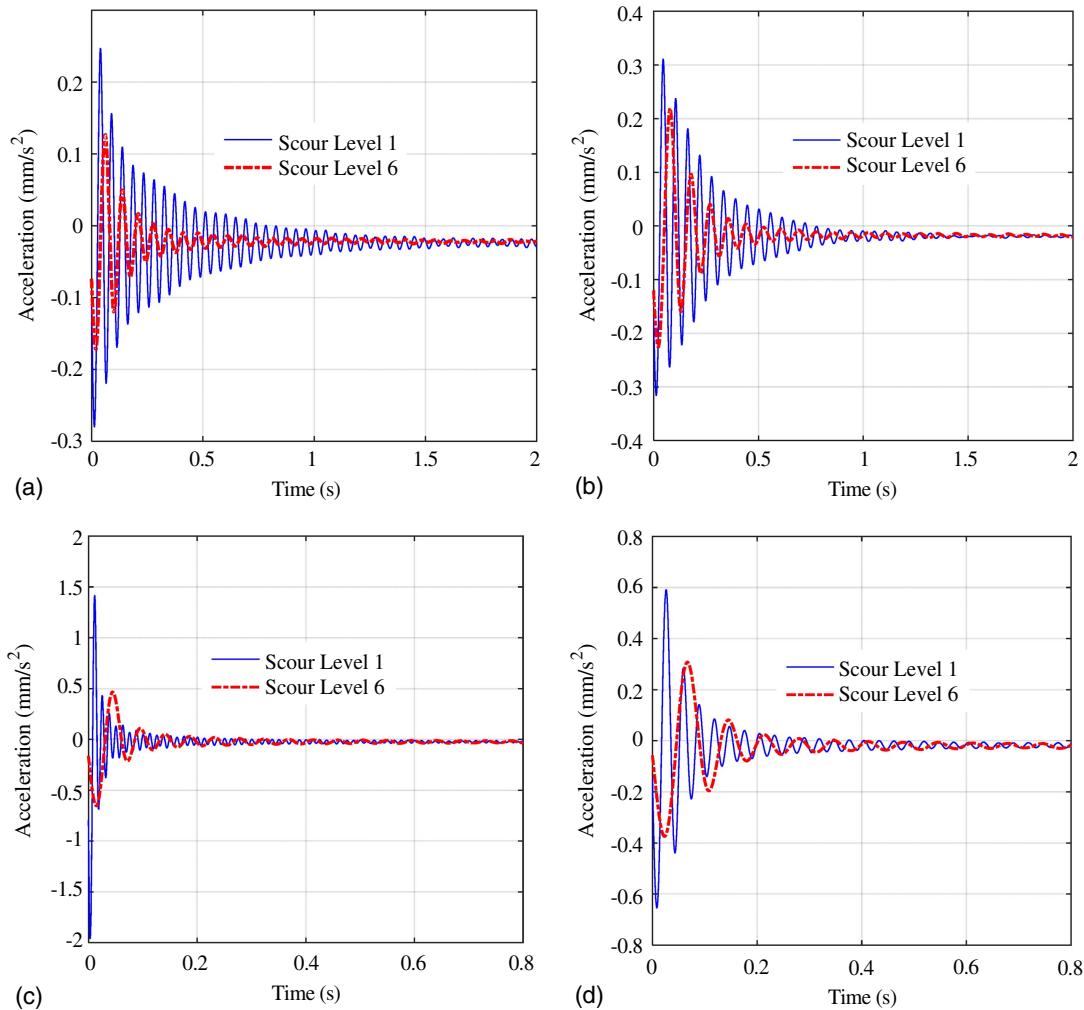


**Fig. 4.** Filtered acceleration: the hollow pipe in the (a) sand; and (b) clay; the concrete column in the (c) sand; and (d) clay.

The springs were gradually removed from the top to the corresponding depth measured in the tests in order to simulate progressive scour. In the following, detailed mathematical descriptions for the previous two SSI formulations are presented.

The dynamic responses of a beam fully embedded in an infinite linear elastic medium can be formulated using the following equation (Wang et al. 2013):

$$\begin{aligned}
 & m\ddot{u} + c\dot{u} + EIu'''' - j\ddot{u}'' + k_0u - k_1u'' \\
 &= p_d - \underbrace{\frac{h}{2}[u'(k_0u - k_1u'')]'}_{\text{quadratic nonlinear term}} - \underbrace{EI[u'(u'')^2 + (u')^2u''']}_{\text{cubic nonlinear term}} \\
 & - \underbrace{\left[\frac{u'}{2} \int_l^x m \frac{\partial^2}{\partial t^2} \int_0^x (u')^2 dx dx\right]'}_{\text{cubic nonlinear term}} \quad (1)
 \end{aligned}$$

where  $u$  = lateral deflection (m);  $\dot{u}$  and  $u'$  denote the first derivative of  $u$  with respect to time and deflection, respectively;  $m$  = mass per unit length (kg/m) with the same cross-section of the beam;  $p_d$  = external distributed load (N/m);  $c$  = damping;  $EI$  = flexural rigidity of the beam (kN m<sup>2</sup>);  $j = \int_{A_c} \rho_b y^2 dA_c$  is the rotary inertia, in which  $A_c$  is the cross-sectional area of the beam (m<sup>2</sup>) and  $\rho_b$  is the beam density (kg/m<sup>3</sup>);  $k_0$  = modulus of subgrade reaction

(N/m<sup>2</sup>); and  $k_1$  = Pasternak parameter (N). The three rightmost terms on the right-hand side of Eq. (1) are nonlinear terms.

By neglecting all nonlinear high-order, damping, and external load terms, the governing equation of the linear undamped free vibration of a beam fully embedded in a semiinfinite linear elastic medium can be written as

$$m\ddot{u} + EIu'''' - j\ddot{u}'' + k_0u - k_1u'' = 0 \quad (2)$$

However, in reality, bridge piers are partially embedded in a soil medium, which cannot be described by Eq. (2) directly. To account for the partially embedded pier, Eq. (2) is therefore rewritten to a piecewise governing equation, where the modulus of subgrade reaction and the Pasternak parameter only exist in the embedded part of the beam [Eq. (3)]

$$m\ddot{u} + EIu'''' - j\ddot{u}'' + k_0u - k_1u'' = 0 \quad 0 \leq x \leq l_s \quad (3)$$

$$m\ddot{u} + EIu'''' - j\ddot{u}'' = 0 \quad l_s \leq x \leq l \quad (4)$$

where  $l_s$  and  $l$  = embedded length (m) and total length (m) of the beam, respectively. If no external load acts on the beam, this beam undergoes free linear vibration. The natural frequency of the beam then can be obtained through the modal analysis of the beam. For this purpose, the general solution to this motion equation can be assumed to be of the form  $u = U_a e^{i\omega t}$ , where  $\omega$  is the angular

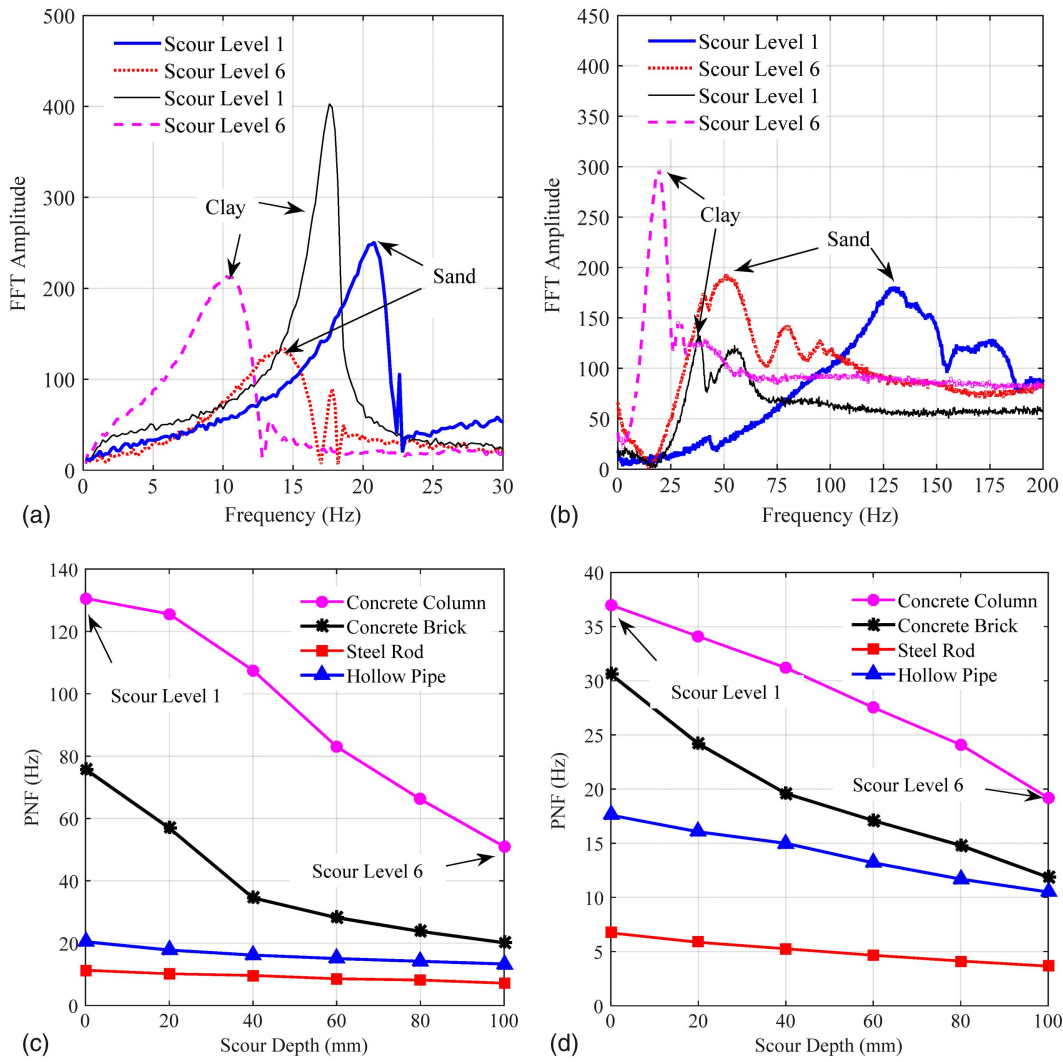


**Fig. 5.** Measured PNFs: (a) unfiltered PNF spectra of the hollow pipe; (b) unfiltered PNF spectra of the concrete column; (c) PNF variations in the sand; and (d) PNF variations in the clay.

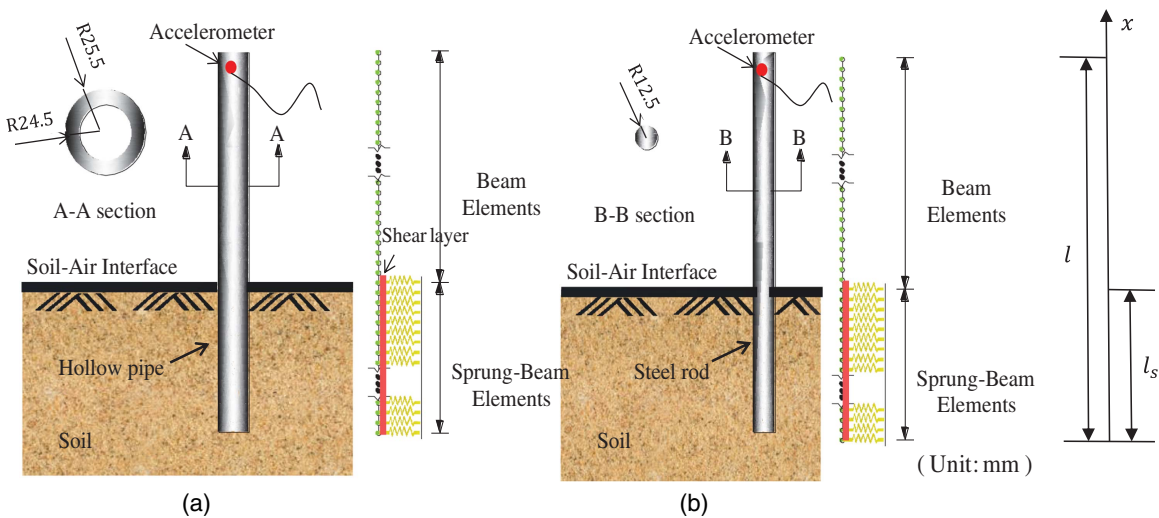


**Fig. 6.** Schematic of discrete springs spaced along the test piers for (a) the hollow pipe; and (b) the steel rod.

natural frequency of the beam and  $U_a$  is the modal shape function. Substituting this solution into Eqs. (3) and (4), one obtains

$$EIU_a'''' - (k_1 - j\omega^2)U_a'' + (k_0 - m\omega^2)U_a = 0 \quad 0 \leq x \leq l_s \quad (5)$$

$$EIU_a'''' + j\omega^2U_a'' - m\omega^2U_a = 0 \quad l_s \leq x \leq l \quad (6)$$

To describe a beam that is partially embedded in a semiinfinite linear elastic medium, the previous piecewise equation is rewritten into the following equation system:

$$EIU'''' - (k_1 - j\omega^2)U'' + (k_0 - m\omega^2)U = 0 \quad 0 \leq x \leq l_s \quad (7)$$

$$EIV'''' + j\omega^2V'' - m\omega^2V = 0 \quad l_s \leq x \leq l \quad (8)$$

where  $U$  = modal shape function in the soil; and  $V$  = modal shape function in the air (no interaction with soil). The previous equations are fourth-order ordinary differential equations. The temporal terms were eliminated to obtain the angular natural frequency  $\omega$ . It can be seen that both Eqs. (7) and (8) are eigenvalue problems, which can be rewritten into a general form of an eigenvalue problem

$$U'''' - \frac{k_1}{EI}U'' + \frac{k_0}{EI}U + \omega^2\left(\frac{j}{EI}U'' - \frac{m}{EI}U\right) = 0 \quad (9)$$

$$V'''' + \omega^2\left(\frac{j}{EI}V'' - \frac{m}{EI}V\right) = 0 \quad (10)$$

Therefore, the natural frequency of the beam  $f$  can be computed simply using  $f = \omega/2\pi$  if the angular natural frequency  $\omega$  is obtained under the specified boundary conditions. According to the lab-scale tests in the "Experiments" section, the boundary conditions of a beam that is partially embedded in a semiinfinite linear elastic medium can be formulated as

$$\text{Embedded part} \begin{cases} U''|_{x=0} = 0 \\ U'''|_{x=0} = 0 \end{cases} \quad (11)$$

$$\text{Continuous} \begin{cases} U|_{x=d} = V|_{x=l_s} \\ U'|_{x=d} = V'|_{x=l_s} \\ U''|_{x=d} = V''|_{x=l_s} \\ U'''|_{x=d} = V'''|_{x=l_s} \end{cases} \quad (12)$$

$$\text{Exposed part} \begin{cases} V''|_{x=l} = 0 \\ V'''|_{x=l} = 0 \end{cases} \quad (13)$$

### Numerical Implementation

Detailed numerical implementations are presented in this section. One simple and efficient numerical strategy to solve Eqs. (9) and (10) with the boundary conditions of Eqs. (11)–(13) is the finite difference method (FDM). The discretization of Eqs. (9) and (10) using the FDM is performed as

$$\delta_x^4 U_i - \frac{k_1}{EI} \delta_x^2 U_i + \frac{k_0}{EI} U_i + \omega^2 \left( \frac{j}{EI} \delta_x^2 U_i - \frac{m}{EI} U_i \right) = 0 \quad (14)$$

$$\delta_x^4 V_i + \omega^2 \left( \frac{j}{EI} \delta_x^2 V_i - \frac{m}{EI} V_i \right) = 0 \quad (15)$$

where  $\delta_x$  = discretization expression of the modal shape function, which is derived using the Taylor series expansion (LeVeque 2007). The derivation is described subsequently in detail.

Applying the Taylor series expansion to the second and fourth derivatives of  $U$  and neglecting the truncation errors, one obtains

$$U'''' \approx \frac{U_{i-2} - 4U_{i-1} + 6U_i - 4U_{i+1} + U_{i+2}}{\Delta x^4} \quad (16)$$

$$U'' \approx \frac{U_{i-1} - 2U_i + U_{i+1}}{\Delta x^2} \quad (17)$$

Substituting Eqs. (16) and (17) into Eq. (9), one obtains the linear equations of the system

$$(A + \omega^2 B)\{U\} = 0 \quad (18)$$

where  $A$  and  $B$  = diagonal matrices and  $\{U\} = [U_{i+1}, U_{i+2}, \dots, U_{n-1}, U_n]^T$ , where  $i$  is the maximum index of  $V$  and  $U$ . Eq. (18) is equivalent to Eq. (14). A similar procedure can be made to obtain linear equations of the system for  $V$  in the air

$$(C + \omega^2 D)\{V\} = 0 \quad (19)$$

where  $C$  and  $D$  = diagonal matrices; and  $\{V\} = [V_1, V_2, \dots, V_i]^T$ .

The incorporation of the boundary conditions of Eqs. (11)–(13) in Eqs. (18) and (19) is crucial for accurately modeling test piers partially embedded in soils. Eq. (13) includes the second and third derivatives of  $V$ . By applying the Taylor series expansion to obtain the discretization of  $V$  in Eq. (13) and substituting them into Eq. (19), one obtains the matrix formulation of Eq. (19) as Eq. (20)

$$\begin{pmatrix} 1 & -2 & 1 & 0 & \dots & 0 \\ -2 & 5 & -4 & 1 & \dots & 0 \\ 1 & -4 & 6 & -4 & \ddots & 0 \\ 0 & 1 & -4 & 6 & \ddots & 1 \\ \vdots & \vdots & \ddots & \ddots & \ddots & -4 \\ 0 & 0 & 0 & 1 & -4 & 6 \end{pmatrix} + \omega^2 \begin{pmatrix} 2CC + DD & 0 & 0 & \dots & 0 & 0 \\ CC & DD & CC & \dots & 0 & 0 \\ 0 & CC & DD & \ddots & 0 & 0 \\ 0 & 0 & CC & \ddots & CC & \vdots \\ \vdots & \vdots & \ddots & \ddots & DD & CC \\ 0 & 0 & 0 & 0 & CC & DD \end{pmatrix} \begin{bmatrix} V_1 \\ V_2 \\ V_3 \\ \vdots \\ V_{i-1} \\ V_i \end{bmatrix} = \mathbf{0} \quad (20)$$

where  $CC = \Delta x^2 j/EI$  and  $DD = -(\Delta x^4 m + 2\Delta x^2 j)/EI$ . Similarly, the boundary condition of Eq. (11) can be implemented into Eq. (18). Thus, the matrix formulation of Eq. (18) is

$$\left( \begin{bmatrix} BB & NN & 1 & 0 & \dots & 0 \\ NN & BB & NN & 1 & \dots & 0 \\ 1 & NN & \ddots & \ddots & \ddots & \vdots \\ \vdots & \ddots & \ddots & BB & NN & 1 \\ 0 & 0 & 1 & NN & BB-1 & 2+NN \\ 0 & 0 & 0 & 1 & -2 & BB+2NN+3 \end{bmatrix} + \omega^2 \begin{bmatrix} DD & CC & 0 & \dots & 0 & 0 \\ CC & DD & CC & \dots & 0 & 0 \\ 0 & CC & DD & \ddots & 0 & 0 \\ 0 & 0 & \ddots & \ddots & CC & \vdots \\ \vdots & \vdots & \ddots & CC & DD & CC \\ 0 & 0 & 0 & 0 & 0 & 2CC+DD \end{bmatrix} \right) \begin{bmatrix} U_{i+1} \\ U_{i+2} \\ U_{i+3} \\ \vdots \\ U_{n-1} \\ U_n \end{bmatrix} = \mathbf{0} \quad (21)$$

where  $BB = 6 + \Delta x^4 k_0/EI - 2\Delta x^2 k_1/EI$  and  $NN = -4 - k_1 \Delta x^2/EI$ . Based on the boundary conditions of Eq. (12), the modal shape at the bottom of the exposed part (in the air), that is,  $V_i$ , is equivalent to that at the top of the embedded part (in the soil), that is,  $U_{i+1}$ , because the test piers are continuous in reality. To achieve this, two steps should be taken to obtain the complete matrix of the system. The first step is to make  $V_i = U_{i+1}$ , which can be achieved by using the same coefficient in the matrix for variables in the lines of  $V_i$  and  $U_{i+1}$ . Second, the coefficients in the matrix for variables in the lines of  $V_{i-1}$  and  $U_{i+2}$  should be rearranged to avoid using  $V_i$  and  $U_{i+1}$  twice because  $V_i = U_{i+1}$ . The diagonal matrix of the whole system including the boundary conditions of Eqs. (11)–(13) is obtained subsequently

$$\left( \begin{bmatrix} 1 & -2 & 1 & 0 & \dots & 0 & \dots & \dots & \dots & \dots & \dots & 0 \\ -2 & 5 & -4 & 1 & \dots & 0 & \ddots & \ddots & \ddots & \ddots & \ddots & \vdots \\ 1 & -4 & 6 & -4 & \ddots & 0 & \dots & \ddots & \ddots & \ddots & \ddots & \vdots \\ 0 & 1 & -4 & 6 & \ddots & 1 & 0 & \dots & \ddots & \ddots & \ddots & \vdots \\ \vdots & \vdots & \ddots & \ddots & \ddots & -4 & 0 & 1 & 0 & \ddots & \ddots & \vdots \\ 0 & 0 & 0 & 1 & NN & BB & 0 & NN & 1 & 0 & \ddots & 0 \\ 0 & \dots & 0 & 1 & NN & 0 & BB & NN & 1 & 0 & \dots & 0 \\ 0 & \ddots & \dots & 0 & 1 & 0 & NN & BB & NN & 1 & \dots & 0 \\ \vdots & \ddots & \ddots & \ddots & \ddots & \ddots & 1 & NN & \ddots & \ddots & \ddots & \vdots \\ \vdots & \ddots & BB & NN & 1 \\ \vdots & \vdots & \ddots & \ddots & \ddots & \ddots & 0 & 0 & 1 & NN & BB-1 & 2+NN \\ 0 & \dots & \dots & \dots & \dots & \dots & 0 & 0 & 0 & 1 & -2 & BB+2NN+3 \end{bmatrix} + \omega^2 \begin{bmatrix} 2CC+DD & 0 & 0 & \dots & 0 & 0 & \dots & \dots & \dots & \dots & \dots & 0 \\ CC & DD & CC & \dots & 0 & 0 & \ddots & \ddots & \ddots & \ddots & \ddots & \vdots \\ 0 & CC & DD & \ddots & 0 & \vdots & \ddots & \ddots & \ddots & \ddots & \ddots & \vdots \\ 0 & 0 & CC & \ddots & CC & 0 & \ddots & \ddots & \ddots & \ddots & \ddots & \vdots \\ \vdots & \vdots & \ddots & \ddots & DD & CC & 0 & \ddots & \ddots & \ddots & \ddots & 0 \\ 0 & 0 & 0 & 0 & CC & DD & 0 & CC & 0 & \ddots & \ddots & 0 \\ 0 & \ddots & \dots & 0 & CC & 0 & DD & CC & 0 & \ddots & \ddots & \vdots \\ \vdots & \ddots & \ddots & \ddots & 0 & 0 & CC & DD & CC & \ddots & \ddots & \vdots \\ \vdots & \ddots & \ddots & \ddots & \ddots & \ddots & 0 & CC & DD & \ddots & \ddots & \vdots \\ \vdots & \ddots & \ddots & \ddots & \ddots & \ddots & \ddots & 0 & \ddots & \ddots & CC & 0 \\ \vdots & \vdots & \ddots & CC & DD & CC \\ 0 & \dots & 0 & 0 & 2CC+DD \end{bmatrix} \right) \begin{bmatrix} V_1 \\ V_2 \\ V_3 \\ \vdots \\ V_{i-1} \\ V_i \\ U_{i+1} \\ U_{i+2} \\ U_{i+3} \\ \vdots \\ U_{n-1} \\ U_n \end{bmatrix} \quad (22)$$

Therefore, a nontrivial solution of Eq. (22) can be obtained for the PNF of the test piers in the experiments. The discretization and eigenvalue solutions were implemented and solved with MATLAB. More details regarding the implementations of boundary conditions of Eqs. (11) and (13) to the diagonal matrices can be referred to in Ansari et al. (2011). The model validation will be detailed later in “Results and Discussion.”

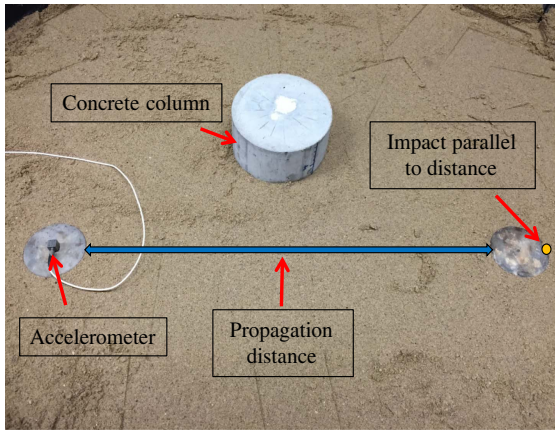


Fig. 7. Geophysical methods for  $E_s$  measurements.

$$k_0 = \frac{1.0E_s}{1 - \nu_s^2} \left[ \frac{E_s D_p^4}{E_p I_p} \right]^{1/12} \quad (24)$$

where  $D_p$  = pier diameter (m); and  $E_p I_p$  = flexural rigidity of the pier ( $\text{kN m}^2$ ).

### APIM Stiffness for Sands

The APIM provides initial subgrade reaction curves with respect to the relative density of sands based on the load-deflection ( $p$ - $y$ ) curves (API 2000) to determine the lateral stiffness of sands. The lateral  $p$ - $y$  relationship for sands is described using the following equation (API 2000):

$$p = A_f p_u \tanh \left[ \frac{kH}{A_f p_u} y \right] \quad (25)$$

where  $p$  = lateral load per unit length of a pier ( $\text{kN/m}$ );  $y$  = lateral deflection (m);  $A_f$  = factor to account for the cyclic or static loading condition;  $p_u$  ( $\text{kN/m}$ ) = ultimate bearing capacity at a certain depth of  $H$ ; and  $k$  = initial modulus of subgrade reaction ( $\text{kN/m}^3$ ), which can be determined based on the relative density of sands. Because a transient lateral impulse force impacting a pier within a very short duration induces very small strains in the sand, the dynamic response of the sand mass on the sand-pier boundary can be represented by differentiating Eq. (25) at  $y = 0$  (Prendergast et al. 2013)

$$\frac{dp}{dy} = \frac{A_f p_u \frac{kH}{A_f p_u}}{\cosh^2 \left( \frac{kH}{A_f p_u} y \right)} \Bigg|_{y=0} = kH \quad (26)$$

Based on that, the lateral stiffness of sands of SSI is given by multiplying  $kH$  in Eq. (26) by the spacing of the adjacent springs at discrete locations along the pier.

### Pasternak Parameter Determination

The Pasternak parameter of the shear layer in Fig. 6 is a crucial parameter for correctly modeling the behavior of the Pasternak SSI. However, the ways to determine the Pasternak parameter are still limited in the existing studies (Breeveld 2013). According to Wang et al. (2013), the Pasternak SSI is independent of the soil depth. Thus, one can determine the Pasternak parameter  $k_1$  using the following equation (Wang et al. 2013):

$$k_1 = \frac{E_0 D_p A_1}{4(1 + \nu_0)\gamma} \quad (27)$$

where  $\nu_0 = \nu_s / (1 - \nu_s)$ ;  $E_0 = E_s / (1 - \nu_s^2)$ ;  $A_1 = \sqrt[3]{2D_b(1 - \nu_0^2) / (E_0 D_p)}$ ;  $D_b = EI / (1 - \nu_b^2)$ , in which  $\nu_s$  and  $\nu_b$  are the Poisson ratios of the soil and the beam, respectively;  $EI$  = flexural rigidity of the beam ( $\text{kN m}^2$ );  $E_s$  = elastic modulus of the soil medium ( $\text{N/m}^2$ ); and  $\gamma$  = attenuation parameter, which was assumed to be 1 in this study according to Wang et al. (2013). The Pasternak SSI can degenerate into the Winkler SSI when  $k_1 = 0$ .

## Results and Discussion

In this section, the lateral stiffness of soils derived from both the SSSM and the APIM for the simulations is presented first. Then, the numerically computed PNFs are compared with the experimentally measured PNFs to evaluate the SSI formulations, that is, the Winkler model and the Pasternak model, in predicting the PNF.

### Soil Lateral Stiffness

The SSSM-based lateral stiffness of soils was calculated using Eq. (24). The real soil behavior for the lateral stiffness, therefore,

### Determination of Soil Stiffness

To correctly model the behavior of SSI, the small-strain stiffness method (SSSM) and the American Petroleum Institute Method (APIM) were used in this study because both yielded good results for the lateral spring stiffness of soils around piers (Prendergast et al. 2013). The SSSM can be used to determine the lateral stiffness of both sands and clays. The lateral stiffness of sands also can be rationally estimated by applying the initial modulus of subgrade reaction in an expression using the APIM according to the API design code (API 2000). However, the APIM was not capable of evaluating the lateral stiffness of clays because of the lack of an existing expression in the API design code.

### SSSM Stiffness for Sands and Clays

A transient lateral dynamic load applied at the top of the pier causes small strains in a soil mass in an ideal test (Atkinson 2000). The SSSM-based soil lateral stiffness is associated with strains of a small order caused by such a transient lateral dynamic loading. The elastic modulus  $E_s$  is a critical parameter in dynamic analyses on the small strain level. To obtain  $E_s$  of soils used in laboratory tests, a geophysical method (Luna and Jadi 2000) was used in this study. As shown in Fig. 7, two metal columns were embedded into the soils (the sand or clay) at a certain wave propagation distance. The velocity of the compression wave in the soil was computed by measuring the difference between the arriving times at the impact point and the point where the signal was received using an accelerometer. In this study,  $E_s$  was assumed to be uniformly distributed within the soils because the soils used in the tests were compacted uniformly. The velocities of the compression wave in the sand and clay matrices were estimated to be 213 and 216 m/s, respectively.

When the velocity of the compression wave was obtained, the  $E_s$  of the soil then could be calculated using the following expression (Luna and Jadi 2000)

$$E_s = \frac{\rho V_c^2 (1 + \nu_s)(1 - 2\nu_s)}{1 - \nu_s} \quad (23)$$

where  $\nu_s$  = small strain Poisson's ratio of soils;  $V_c$  = compression wave velocity (m/s); and  $\rho$  = density of soils ( $\text{kg/m}^3$ ).

The relationship between the modulus of subgrade reaction  $k_0$  and the other basic material properties in the elastic continuum is given by Eq. (24) (Ashford and Juimarongrit 2003). The lateral spring stiffness thus can be determined by multiplying  $k_0$  ( $\text{kN/m}^2$ ) by the spacing of the adjacent springs

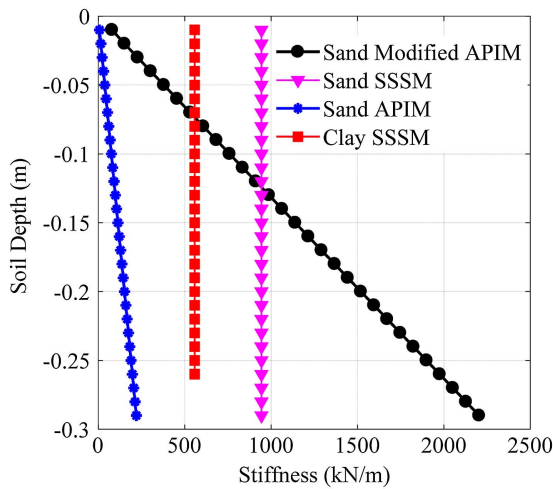


**Fig. 8.** Stiffness of springs used in numerical simulations for the hollow pipe.

can be obtained accurately if  $E_s$  is precisely measured. Fig. 8 shows the lateral stiffness for the sand computed using the APIM and for the sand and clay calculated using the SSSM. In the API code,  $k$  is estimated based on the relative density of sands, whereas the maximum  $k$  by default in the API code can only be estimated at a relative density of 80%. Because of this, the APIM-based lateral stiffness

may fail to reflect the real situation (almost 100% relative density) in the laboratory tests by underestimating the lateral stiffness. This can also be seen from the comparison between the SSSM and APIM stiffnesses for the sand in Fig. 8. The APIM stiffness estimated using a relative density of 80% is much lower than the SSSM stiffness. The SSSM stiffness could be accurate because it is computed based on the parameters of the soils tested experimentally. The APIM stiffness should be comparable to the SSSM stiffness. Because the APIM stiffness increases with the soil depth, one way to solve this problem is that the average of the APIM stiffness is comparable to the SSSM stiffness. Therefore,  $k$  was multiplied by 5 to obtain a reasonable APIM stiffness in the simulations. A similar treatment to obtain the reasonable APIM stiffness was also done in Prendergast et al. (2013).

### Validation and Evaluation

The computed PNFs were compared with the measured PNFs to validate the numerical model and also to evaluate the Winkler and Pasternak SSIs for PNF prediction. In the sand, as shown in Fig. 9(a), the PNFs of the hollow pipe obtained using both the SSSM-based and APIM-based lateral stiffness calculated using the Winkler SSI agreed very well with the experimental data. This also happened with the steel rod, as shown in Fig. 9(c), though the computed PNFs were slightly higher than the measured PNFs. The major reason for this slight error in the computed PNFs is that the measured PNFs are lower than those in an ideal test. This is because

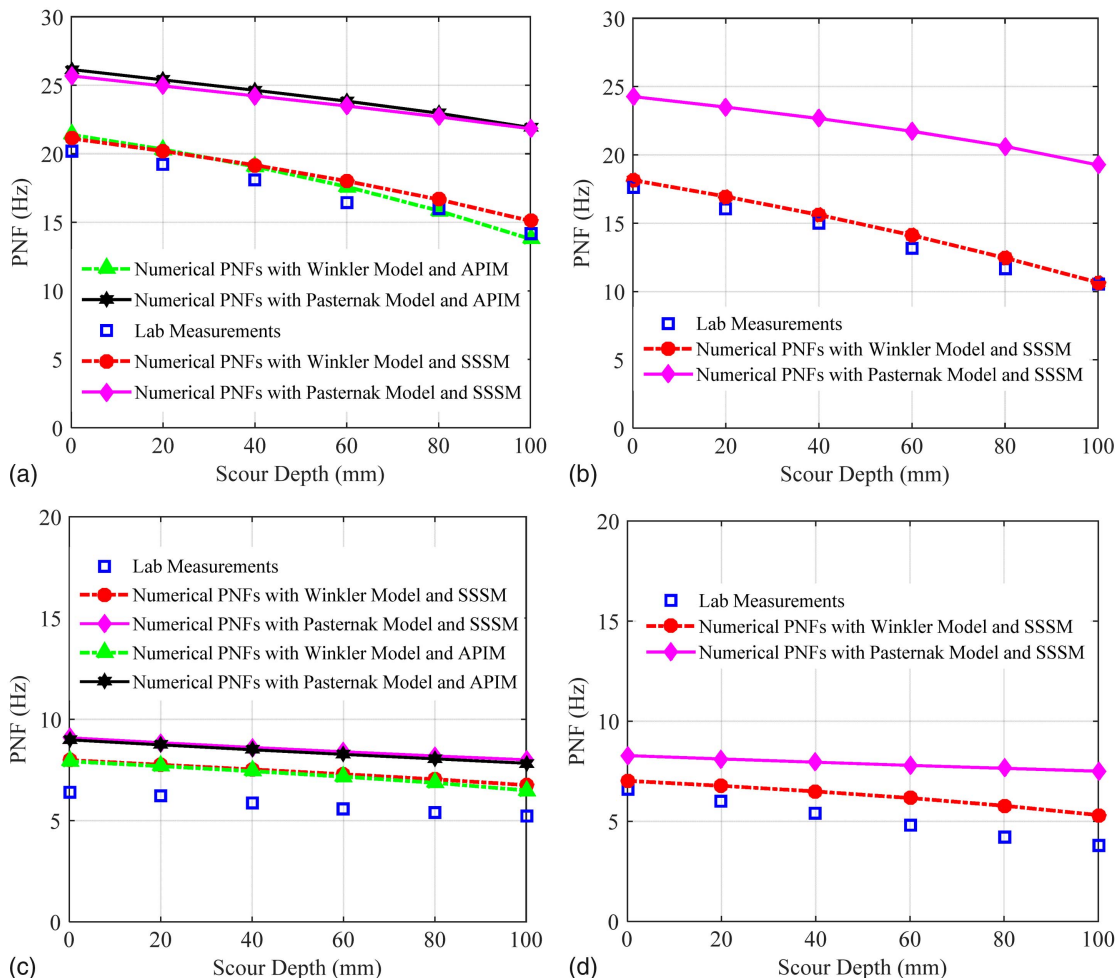


**Fig. 9.** PNF comparisons: (a) hollow pipe in the sand; (b) hollow pipe in the clay; (c) steel rod in the sand; and (d) steel rod in the clay.

the embedded length of the steel rod was very small compared to its total length, and consequently, the free vibration generated by the modal hammer resulted in a small gap between the soil and the steel rod at locations close to the soil surface. This led to low PNFs in the measurement. However, the springs used to simulate soils around the pier interacted with the pier in an ideal condition, leading to computed PNFs that were higher than the measured PNFs. Because of this, the computed PNFs of the steel rod in Figs. 9(c and d) were higher than the measured PNFs.

However, when the Pasternak parameter was taken into account, the computed PNFs were higher than the measured PNFs for both the hollow pipe (about 24%) and steel rod (about 38%), as illustrated in Figs. 9(a and c), either using the SSSM-based or APIM-based lateral stiffness. For the piers measured in the clay, values about 39% higher for the hollow pipe and about 31% higher for the steel rod were obtained when the Pasternak parameter was taken into account, as shown in Figs. 9(b and d). The PNFs of both the hollow pipe and steel rod calculated using the Winkler SSI were in very good agreement with the experimental data. However, when the Pasternak parameter was not equal to zero, the computed PNFs were higher than the measured PNFs.

The comparison between the measured and computed PNFs in Fig. 9 reveals that the Winkler SSI yielded better results than the Pasternak SSI. To further prove this, the field test data measured by Prendergast et al. (2013) for an idealized pier with more realistic dimensions were compared with the computed PNFs using the framework developed in this study. Prendergast et al. (2013) carried out a field-scale test using an idealized pier with a length of 8.75 m partially embedded in a dense sand site with a focus on detecting the change in the PNF affected by scour progression. Based on the soil properties measured in Prendergast et al. (2013), the PNF of this field-scale pier was computed using 30 sprung-beam elements (sprung-shear layer-beam elements for the Pasternak model) and 10 beam elements (each 219 mm long). The soil lateral stiffness was calculated using the SSSM.

As shown in Fig. 10, the Winkler PNF decreased from 31.8 to 1.0 Hz with the increase of the scour depth, which matches very well with the measured PNFs in the field test (Prendergast et al. 2013) decreasing from 31.7 to 2.1 Hz. However, the Pasternak PNFs were higher than the Winkler and field-scale measured PNFs. This difference was significant in the low scour depth range (0–2 m). With the

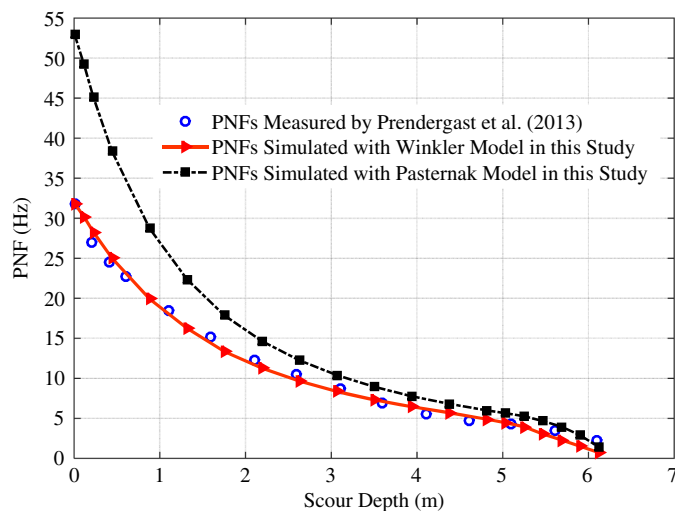


**Fig. 10.** PNF comparison between computed PNFs and field data measured by Prendergast et al. (2013).

progression of scour, the Pasternak PNFs greatly decreased to be close to the Winkler PNFs and the field-scale measured PNFs in the high scour depth range (4–6 m). The reason for this is that the shear interaction of springs decreases with scour progression. In this high scour depth range, the shear interaction is less significant and the system begins to act more like a loosely constrained cantilever because of limited SSI as a result of the small soil depth in contact. However, it can also be seen that the Pasternak PNFs were still higher than the Winkler and measured PNFs in this high scour depth range, which is similar to what was concluded from Fig. 9.

Based on the results in Figs. 9 and 10, the Winkler SSI formulation is a better option to formulate SSI in predicting the PNF of an idealized pier partially embedded in an elastic foundation. The Pasternak SSI formulation fails to correctly simulate the situation because of the previous deviations. This finding is different from those obtained in the dynamic response of structures resting on an elastic foundation (i.e., not partially embedded). For example, Valsangkar and Pradhanang (1988) obtained more realistic results for the dynamic response of structures with the Pasternak model by considering the continuity of foundation media via the shear interaction, which is not considered in the Winkler model. Also, Wang et al. (2014) found that the Pasternak model is more accurate than the Winkler model to analyze the dynamic responses of pile fully embedded in soils. In addition, Wang et al. (2013) concluded that the PNF (i.e., first frequency) of structures resting on the Pasternak foundation is slightly lower (about 0.1%) than that on the Winkler foundation, which is also different from the results obtained in this study that Pasternak PNFs are higher than Winkler PNFs of a structure partially embedded in the soil.

This different finding is primarily attributable to two facts. First, the PNF corresponds to the first mode shape of a beam in its free vibration. The deformed pattern of a beam corresponding to the first mode shape is the lateral bending in the case of a free-free beam considered in this study. When a beam rests on the Winkler foundation considered in the existing studies, the lateral deformation corresponding to the first mode shape shears the Winkler springs. However, the Winkler springs are mainly used to resist a compressive force rather than a shearing force. Therefore, the Pasternak foundation could yield more realistic PNF predictions by adding the shear interaction between soil springs. This is different from the situation discussed in this study, where a beam is partially embedded in the Winkler foundation. This is because the lateral bending corresponding to the first mode shape compresses rather than shears the Winkler springs. Therefore, adding the shear interaction between soil springs further increases the strength of the Winkler SSI, leading to an overestimation of the predicted PNFs. Second, the previous high deviations for the computed PNFs using the Pasternak SSI formulation may be affected by the Pasternak parameter  $k_1$  calculated using Eq. (27). There are a few ways in the literature to determine the Pasternak parameter (Breeveld 2013), especially for the lateral free vibration of a beam partially embedded in soils involving the Pasternak SSI. As indicated by Eq. (27), the soil's elastic modulus mainly determines the Pasternak parameter. Such a parameter linearly varies with changes in the soil's elastic modulus. This linear variation, however, might cause unreasonable predictions for PNFs of beams partially embedded in the Pasternak foundation. Therefore, further research is required to provide more in-depth discussion on the finding obtained in this study. Also, the water content affects the PNF by influencing the soil's elastic modulus to determine the strength of SSI (Lu and Murat 2013), depending on soil types. Future work thus is needed to further consider the water table effect, especially for clays and silts, to more comprehensively evaluate the performance of the two models adopted in this study.

## Conclusions

This paper presents a comprehensive study to evaluate two predominant soil-structure interaction formulations, that is, the Winkler model and the Pasternak model, for dynamic modeling in the prediction of the PNFs of structures partially embedded in soils. The evaluation was carried out with a significant application: PNF-based bridge scour detection, a non-destructive testing technique that has been gaining increasing attention. Lab-scale tests were conducted first using idealized piers partially embedded in two major types of soils, that is, a sand (less cohesive) and a clay (cohesive), to consider two major representative SSI scenarios at most bridges. Then, a numerical framework for an idealized beam partially embedded in a semiinfinite linear elastic medium was developed. The implementations and discretization of the framework were presented in detail, which have not been reported in the literature before. The numerical results were then compared with the experimental data to evaluate the SSI formulations for the PNF prediction.

The comparison between the computed and measured PNFs indicated that the Winkler SSI formulation yields a better PNF prediction when compared with the Pasternak model, regardless of the types of test piers and soils. The Pasternak PNFs are about 24%–38% and 31%–39% higher than the Winkler and measured PNFs, respectively. When compared with documented results for a more realistic field test, the difference between the Pasternak and measured PNFs from this documented test was significant in the small scour depth range, whereas the Pasternak PNFs approached the Winkler and field-scale measured PNFs in the high scour depth range. This is because the shear interaction of springs decreases with scour progression. However, the Pasternak PNFs are still higher than the Winkler and measured PNFs in the high scour depth range. This finding from the previous comparisons is different from those obtained in the dynamic response of structures resting on or fully embedded in an elastic foundation (i.e., not partially embedded), where the Pasternak model can represent more realistic soil conditions compared with the Winkler model by overcoming the limitation of the Winkler model without considering the continuity of the nature of foundation media. Based on the results obtained in this study, it is recommended to use the Winkler SSI for dynamic modeling in predicting the PNF for soil-structure systems where the structure is partially embedded in the soil.

## References

- Ansari, R., R. Gholami, and K. Hosseini. 2011. "A sixth-order compact finite difference method for free vibration analysis of Euler-Bernoulli beams." *Math. Sci.* 5 (4): 307–320.
- API (American Petroleum Institute). 2000. *Recommended practice for planning, designing and constructing fixed offshore platforms-working stress design*. Washington, DC: API.
- Ashford, S. A., and T. Juimarongrit. 2003. "Evaluation of pile diameter effect on initial modulus of subgrade reaction." *J. Geotech. Geoenviron. Eng.* 129 (3): 234–242. [https://doi.org/10.1061/\(ASCE\)1090-0241\(2003\)129:3\(234\)](https://doi.org/10.1061/(ASCE)1090-0241(2003)129:3(234)).
- Atkinson, J. 2000. "Non-linear soil stiffness in routine design." *Geotechnique* 50 (5): 487–508. <https://doi.org/10.1680/geot.2000.50.5.487>.
- Bao, T., and Z. Liu. 2016. "Vibration-based bridge scour detection: A review." *Struct. Control Health Monit.* 24 (7): 1–19. <https://doi.org/10.1002/stc.1937>.
- Bao, T., R. A. Swartz, S. Vitton, Y. Sun, C. Zhang, and Z. Liu. 2017. "Critical insights for advanced bridge scour detection using the natural frequency." *J. Sound Vib.* 386 (Jan): 116–133. <https://doi.org/10.1016/j.jsv.2016.06.039>.
- Breeveld, B. J. S. 2013. *Modelling the interaction between structure and soil for shallow foundations*, 1–115. Rotterdam, Netherlands: Delft Univ. of Technology.
- Chen, W., C. Lü, and Z. Bian. 2004. "A mixed method for bending and free vibration of beams resting on a Pasternak elastic foundation." *Appl. Math. Modell.* 28 (10): 877–890. <https://doi.org/10.1016/j.apm.2004.04.001>.
- Cox, W. R., L. C. Reese, and B. R. Grubbs. 1974. "Field testing of laterally loaded piles in sand." In *Proc., Offshore Technology Conf.*, 1–14. Houston: Offshore Technology Conference.
- De Rosa, M. 1995. "Free vibrations of Timoshenko beams on two-parameter elastic foundation." *Comput. Struct.* 57 (1): 151–156. [https://doi.org/10.1016/0045-7949\(94\)00594-S](https://doi.org/10.1016/0045-7949(94)00594-S).
- De Rosa, M., and M. Maurizi. 1998. "The influence of concentrated masses and Pasternak soil on the free vibrations of Euler beams—Exact solution." *J. Sound Vib.* 212 (4): 573–581. <https://doi.org/10.1006/jsvi.1997.1424>.
- Dutta, S. C., and R. Roy. 2002. "A critical review on idealization and modeling for interaction among soil-foundation-structure system." *Comput. Struct.* 80 (20): 1579–1594. [https://doi.org/10.1016/S0045-7949\(02\)00115-3](https://doi.org/10.1016/S0045-7949(02)00115-3).
- Far, H., B. Fatahi, and B. Samali. 2013. "Seismic behavior of building frames considering dynamic soil-structure interaction." *Int. J. Geomech.* 13 (4): 409–420. [https://doi.org/10.1061/\(ASCE\)GM.1943-5622.0000231](https://doi.org/10.1061/(ASCE)GM.1943-5622.0000231).
- Foti, S., and D. Sabia. 2011. "Influence of foundation scour on the dynamic response of an existing bridge." *J. Bridge Eng.* 16 (2): 295–304. [https://doi.org/10.1061/\(ASCE\)BE.1943-5592.0000146](https://doi.org/10.1061/(ASCE)BE.1943-5592.0000146).
- Gerolymos, N., and G. Gazetas. 2006. "Winkler model for lateral response of rigid caisson foundations in linear soil." *Soil Dyn. Earthquake Eng.* 26 (5): 347–361. <https://doi.org/10.1016/j.soildyn.2005.12.003>.
- Huang, X., L. He, and G. Ma. 2011. "Soil-structure interaction and pulse shape effect on structural element damage to blast load." *J. Perform. Constr. Facil.* 25 (5): 400–410. [https://doi.org/10.1061/\(ASCE\)CF.1943-5509.0000229](https://doi.org/10.1061/(ASCE)CF.1943-5509.0000229).
- Hussien, M. N., S. Iai, and M. Karray. 2018. "Analysis of characteristic frequencies of coupled soil-pile-structure systems." *Int. J. Geomech.* 18 (6): 04018047. [https://doi.org/10.1061/\(ASCE\)GM.1943-5622.0001145](https://doi.org/10.1061/(ASCE)GM.1943-5622.0001145).
- Ju, S. 2013. "Determination of scoured bridge natural frequencies with soil-structure interaction." *Soil Dyn. Earthquake Eng.* 55 (Dec): 247–254. <https://doi.org/10.1016/j.soildyn.2013.09.015>.
- Ko, Y., W. Lee, W. Chang, H. Mei, and C. Chen. 2010. "Scour evaluation of bridge foundations using vibration measurement." In *Proc., 5th Int. Conf. on Scour and Erosion*, 884–893. Reston, VA: ASCE.
- Lee, J. K., S. Jeong, and J. Lee. 2014. "Natural frequencies for flexural and torsional vibrations of beams on Pasternak foundation." *Soils Found.* 54 (6): 1202–1211. <https://doi.org/10.1016/j.sandf.2014.11.013>.
- LeVeque, R. J. 2007. *Finite difference methods for ordinary and partial differential equations: Steady-state and time-dependent problems*. Philadelphia: Society for Industrial and Applied Mathematics.
- Liu, Z., G. Cui, and X. Wang. 2014. "Vibration characteristics of a tunnel structure based on soil-structure interaction." *Int. J. Geomech.* 14 (4): 04014018. [https://doi.org/10.1061/\(ASCE\)GM.1943-5622.0000357](https://doi.org/10.1061/(ASCE)GM.1943-5622.0000357).
- Lombardi, D., S. Bhattacharya, and D. M. Wood. 2013. "Dynamic soil-structure interaction of monopile supported wind turbines in cohesive soil." *Soil Dyn. Earthquake Eng.* 49 (Jun): 165–180. <https://doi.org/10.1016/j.soildyn.2013.01.015>.
- Lu, N., and K. Murat. 2013. "Power law for elastic moduli of unsaturated soil." *J. Geotech. Geoenviron. Eng.* 140 (1): 46–56. [https://doi.org/10.1061/\(ASCE\)GT.1943-5606.0000990](https://doi.org/10.1061/(ASCE)GT.1943-5606.0000990).
- Luna, R., and H. Jari. 2000. "Determination of dynamic soil properties using geophysical methods." In *Proc., 1st Int. Conf. on the Application of Geophysical and NDT Methodologies to Transportation Facilities and Infrastructure-Geophysics*, 1–15. Washington, DC: Transportation Research Board of the National Academies.
- Matlock, H. 1970. "Correlations for design of laterally loaded piles in soft clay." In Vol. 1204 of *Proc., Offshore Technology in Civil Engineering's Hall of Fame Papers from the Early Years*, 77–94. Houston: Offshore Technology Conference.
- Prendergast, L. J., and K. Gavin. 2016. "A comparison of initial stiffness formulations for small-strain soil-pile dynamic Winkler modelling."

- Soil Dyn. Earthquake Eng.* 81 (Feb): 27–41. <https://doi.org/10.1016/j.soildyn.2015.11.006>.
- Prendergast, L. J., D. Hester, K. Gavin, and J. J. O’Sullivan. 2013. “An investigation of the changes in the natural frequency of a pile affected by scour.” *J. Sound Vib.* 332 (25): 6685–6702. <https://doi.org/10.1016/j.jsv.2013.08.020>.
- Reese, L. C., and R. C. Welch. 1975. “Lateral loading of deep foundations in stiff clay.” *J. Geotech. Eng. Div.* 101 (7): 633–649.
- Roy, P. K., and N. Ganesan. 1995. “Transient response of a cantilever beam subjected to an impulse load.” *J. Sound Vib.* 183 (5): 873–880. <https://doi.org/10.1006/jsvi.1995.0291>.
- Shinoda, M., H. Haya, and S. Murata. 2008. “Nondestructive evaluation of railway bridge substructures by percussion test.” In *Proc., 4th Int. Conf. on Scour and Erosion*, 285–290. London: International Society for Soil Mechanics and Foundation Engineering.
- Taghavi, A., and K. K. Muraleetharan. 2016. “Analysis of laterally loaded pile groups in improved soft clay.” *Int. J. Geomech.* 17 (4): 1–13. [https://doi.org/10.1061/\(ASCE\)GM.1943-5622.0000795](https://doi.org/10.1061/(ASCE)GM.1943-5622.0000795).
- Valsangkar, A., and R. Pradhanang. 1988. “Vibrations of beam-columns on two-parameter elastic foundations.” *Earthquake Eng. Struct. Dyn.* 16 (2): 217–225. <https://doi.org/10.1002/eqe.4290160205>.
- Wang, C., Y. Xiang, and Q. Wang. 2001. “Axisymmetric buckling of Reddy circular plates on Pasternak foundation.” *J. Eng. Mech.* 127 (3): 254–259. [https://doi.org/10.1061/\(ASCE\)0733-9399\(2001\)127:3\(254\)](https://doi.org/10.1061/(ASCE)0733-9399(2001)127:3(254)).
- Wang, J., D. Zhou, T. Ji, and S. Wang. 2017. “Horizontal dynamic stiffness and interaction factors of inclined piles.” *Int. J. Geomech.* 17 (9): 04017075. [https://doi.org/10.1061/\(ASCE\)GM.1943-5622.0000966](https://doi.org/10.1061/(ASCE)GM.1943-5622.0000966).
- Wang, J., D. Zhou, and W. Liu. 2014. “Horizontal impedance of pile groups considering shear behavior of multilayered soils.” *Soils Found.* 54 (5): 927–937. <https://doi.org/10.1016/j.sandf.2014.09.001>.
- Wang, L., J. Ma, Y. Zhao, and Q. Liu. 2013. “Refined modeling and free vibration of inextensional beams on the elastic foundation.” *J. Appl. Mech.* 80 (4): 1–11.
- Yokoyama, T. 1991. “Vibrations of timoshenko beam-columns on two-parameter elastic foundations.” *Earthquake Eng. Struct. Dyn.* 20 (4): 355–370. <https://doi.org/10.1002/eqe.4290200405>.